Creep–Fatigue Interaction Effects on Pressure-Reducing Valve Under Cyclic Thermomechanical Loadings Using Direct Cyclic Method

Nak-Kyun Cho[1]
Department of Manufacturing Systems and Design Engineering,
Seoul National University of Science and Technology,
Seoul 01811, South Korea
e-mail: nkcho@seoultech.ac.kr

Youngjae Choi
Department of Manufacturing Systems and Design Engineering,
Seoul National University of Science and Technology,
Seoul 01811, South Korea

Haofeng Chen
Department of Mechanical and Aerospace Engineering,
University of Strathclyde,
Glasgow G1 1XJ, UK

Supercritical boiler system has been widely used to increase efficiency of electricity generation in power plant industries. However, the supercritical operating condition can seriously affect structural integrity of power plant components due to high temperature that causes degradation of material properties. Pressure reducing valve is an important component being employed within a main steam line of the supercritical boiler, which occasionally thermal-fatigue failure being reported. This research has investigated creep-cyclic plastic behavior of the pressure reducing valve under combined thermomechanical loading using a direct numerical method known as extended direct steady cycle analysis of the linear matching method framework (LMM eDSCA). Finite element model of the pressure-reducing valve is created based on a practical valve dimension and temperature-dependent material properties are applied for the numerical analysis. The simulation results demonstrate a critical loading component that attributes creep-fatigue failure of the valve. Parametric studies confirm the effects of magnitude of the critical loading component on creep deformation and total deformation per loading cycle. With these comprehensive numerical results, this research provides engineer with an insight into possible failure mechanisms of the pressure-reducing valve at high temperature.
[DOI: 10.1115/1.4052658]

Keywords: pressure reducing valve, creep, cyclic plasticity, the linear matching method, supercritical boiler

1 Introduction

Conventional power plants generate electricity with turbines powered by hot steam generated from boiler system. After centuries of development, a supercritical boiler system was developed and now frequently used at commercial power plants, since it can generate the electricity more efficiently with superheated steam [1]. One of crucial parts of a supercritical boiler system is a pressure-reducing valve (PRV) that places at the main-steam pipe line, and reduces high temperature and pressure of the superheated steam before it flows into startup vessel (SUV). Considering the harsh operating condition of PRV, it requires to be designed securing a high level of safety against potential accidents such as crack initiation caused by creep-fatigue damage.

For such components subjected to complex cyclic loading at the high temperature, it is hard to predict structural behaviors that involves inelastic strains accumulated in combination of creep and plastic deformation over every cyclic loading. In addition, two typical phenomenon, creep and stress relaxation, observed from materials at high temperature can have significant impacts on the structural integrity with creep-fatigue interaction [2,3]. Industry standards such as R5 procedures [4], ASME NH code [5], and RCC-MRx [6] are commonly used in safety cases for structural integrity assessment of high temperature component. However, theses rule based methods predict overly conservative structural behaviors, leading to short life expectancy. Moreover it is not eligible for a structure exhibiting complicated stress–strain behaviors. For such cases, the standards also recommend to conduct detailed structural integrity assessment of high temperature component considering temperature dependent material behaviors using inelastic finite element (FE) analysis.

FE based analysis have been developed and improved greatly, especially direct methods have demonstrated that it can balance between time-efficiency and accuracy compared to the time-consuming step by step analysis. One of well-known direct methods is the linear matching method framework (LMMF) that analyze cyclic plastic behavior such as shakedown and ratchetting [7,8]. The LMMF also include an augmented numerical procedure called extended direct stress cycle analysis (eDSCA) that can analyze cyclic structural response considering creep-fatigue interaction [9]. Recently, application of eDSCA has been extended to predicting creep-fatigue interaction with temperature dependent creep properties and capable of calculating creep-fatigue damage using different damage models [10]. Over the past decade, the LMMF have been utilized to analyze complicated structural problems that involve, especially, high temperature [11–13]. Hence, this research has conducted to evaluate structural behavior of PRV with the modified eDSCA method.

Cho et al. Presented a cyclic plastic behavior of the PRV under cyclic thermomechanical loading but creep effects was not considered [14]. The objective of this research is to analyze the creep cyclic plasticity behavior of the PRV subjected to complex cyclic thermomechanical loadings that comprised of cyclic system moments (in-plane, out-of-plane, and torsion), cyclic internal pressure, and cyclic thermal loads. The effect of individual system moment and of combined system moment level on both creep and plastic deformation are investigated. Numerical results exhibit factors to affect those structural integrity of the PRV and causes

[1]Corresponding author.

Contributed by the Pressure Vessel and Piping Division of ASME for publication in the Journal of Pressure Vessel Technology. Manuscript received December 28, 2020; final manuscript received September 30, 2021; published online November 8, 2021. Assoc. Editor: Catrin Davies.

are discussed. Based on findings, this research provides insight into possible failure mechanism of the PRV at high temperature.

This paper structures as follows. Section 2 describes numerical procedures of the LMM eDSCA. Section 3 provides the problem descriptions of this research such as finite element model created for the analysis, material properties used and parameters considered for this numerical analysis. The numerical results and discussions are presented in the Sec. 4. Finally, Sec. 5 concludes this research.

2 Direct Steady Cycle Analysis Method

Creep cyclic plastic behavior of the pressure-reducing valve is assessed using an extended direct steady cycle analysis (eDSCA) method of the linear matching method framework [9]. The eDSCA procedure calculates the cyclic stress history at the steady cycle state in associated with residual stresses accumulated by inelastic strains either plastic or creep during the loading cycle. The eDSCA utilize a minimization procedure that has an assumption that plastic strain only occurs at time t_n, where N (from $n=1$ to N) denotes total number of loading instances. The minimization function of the eDSCA in an incremental form can be given by Eq. (1).

$$I^n\left(\Delta\varepsilon_{ij}^n\right) = \int_V \left\{\sigma_{ij}^n \Delta\varepsilon_{ij}^n - \left[\hat{\sigma}_{ij}(t_n) + \rho_{ij}^r(t_n)\right]\Delta\varepsilon_{ij}^n\right\} dV \geq 0 \quad (1)$$

By an iterative process, the strain increment $\Delta\varepsilon_{ij}^n$ can be calculated by the minimization process until the requested a total number of cycles M. The number of load instances N is performed as subcycles within each cycle m, where m (from $m=1$ to M). Hence, the accumulated residual stress for nth load instance at mth cycle of iterations can be expressed by Eq. (2).

$$\rho_{ij}^r(t_n)_m = \sum_{i=1}^{m-1}\sum_{n=1}^{N} \Delta\rho_{ij}^r(t_n)_i + \sum_{i=1}^{n} \Delta\rho_{ij}^r(t_i)_m \quad (2)$$

For example, if the cycles m and $m+1$ are only considered, the iterative shear modulus $\bar{\mu}_n(t_n)$ at a load instance t_n can be defined by Eq. (3), where $\sigma_y(t_n)_m$ denotes the von-Mises yield stress of the elastic perfectly plastic model, which is substituted to creep flow stress $\bar{\sigma}_c$ when the t_n involves a load instance of creep.

$$\bar{\mu}_{m+1}(t_n) = \bar{\mu}_m(t_n)\frac{\sigma_y(t_n)_m}{\bar{\sigma}(\hat{\sigma}_{ij}(t_n) + \rho_{ij}^r(t_n)_m} \quad (3)$$

Without consideration of a load instance of creep, the inelastic strain increment $\Delta\varepsilon_{ij}^n(t_n)_{m+1}$ at the cycle $m+1$ can be calculated by Eq. (4), where $\rho_{ij}^r(t_{n-1})$ is the accumulated previous residual stress before the time t_n and the notation (') refers to the deviatoric component:

$$\Delta\varepsilon_{ij}(t_n)'_{m+1} = \frac{1}{2\bar{\mu}_m(t_n)}\left\{\hat{\sigma}_{ij}(t_n) + \Delta\rho_{ij}^r(t_{n-1})_{m+1} + \Delta\rho_{ij}^r(t_n)_{m+1}\right\}' \quad (4)$$

where the residual stress accumulated at the cycle m is the summation of the previous varying residual stress and constant residual stress.

$$\rho_{ij}^r(t_{n-1})_m = \rho_{ij}^r(t_0) + \Delta\rho_{ij}^r(t_1) + \Delta\rho_{ij}^r(t_2) + \cdots + \Delta\rho_{ij}^r(t_{n-1}) \quad (5)$$

To calculate creep strain accumulated during a dwell period, time hardening power law shown in Eq. (6) is used to calculate creep deformation, where $\dot{\bar{\varepsilon}}^c$ is the effective creep strain rate; $\bar{\sigma}$ is the von-Mises stress, t is the dwell time; A, n, and m are creep constants.

$$\dot{\bar{\varepsilon}}^c = A \cdot \bar{\sigma}^n \cdot t^m \quad (6)$$

It is assumed that the stress relaxation process follows a linear relation that has been generally defined as Eq. (7) with an elastic follow-up factor Z, where $\bar{E}$ is the effective modulus of elasticity which can be defined as $\bar{E} = 3E/2(1+\upsilon)$; E is the modulus of elasticity; υ is the Poisson's ratio; $\dot{\bar{\sigma}} = \dot{\bar{\sigma}}(\sigma_{ij})$.

$$\dot{\bar{\varepsilon}}^c = -\frac{Z}{\bar{E}}\dot{\bar{\sigma}} \quad (7)$$

Equations (6) and (7) are combined and then integrated the combined equation over the dwell time Δt:

$$\frac{A\bar{E}\Delta t^{m+1}}{Z(m+1)} = \frac{1}{n-1}\left(\frac{1}{\bar{\sigma}_c^{-n+1}} - \frac{1}{\bar{\sigma}_s^{-n+1}}\right) \quad (8)$$

where $\bar{\sigma}_s$ is the start of the dwell stress; $\bar{\sigma}_c$ is the end of the dwell stress (creep flow stress) which replace the $\sigma_y(t_n)_m$ in Eq. (3) within the iterative process. Integrating Eq. (7) over the dwell time Δt and then combined with Eq. (8) to eliminate $Z/\bar{E}$, where $\Delta\bar{\varepsilon}^c$ is the effective creep strain increment over the dwell time.

$$\Delta\bar{\varepsilon}^c = \frac{A(n-1)\Delta t^{m+1}(\bar{\sigma}_s - \bar{\sigma}_c)}{(\bar{\sigma}_c^{-n+1} - \bar{\sigma}_s^{-n+1})(m+1)} \quad (9)$$

The creep strain rate $\dot{\bar{\varepsilon}}^c$ at the end of the dwell time Δt is calculated from Eqs. (8) and (9).

$$\dot{\bar{\varepsilon}}^c = \frac{\Delta\bar{\varepsilon}^c(m+1)\bar{\sigma}_c^n}{(n-1)(\bar{\sigma}_s - \bar{\sigma}_c)\Delta t}\left(\bar{\sigma}_c^{-n+1} - \bar{\sigma}_s^{-n+1}\right) \quad (10)$$

Initially the iterative process starts with estimated $\bar{\sigma}_s$ and $\bar{\sigma}_c$ values and the Eqs. (9) and (10) compute new creep flow stress $\bar{\sigma}_c^f$ using Eq. (11), so that the $\bar{\sigma}_c^f$ replace $\sigma_y(t_n)_m$ in Eq. (3) to carry out the linear matching condition.

$$\bar{\sigma}_c^f = \left(\frac{\dot{\bar{\varepsilon}}^c}{A\Delta t^m}\right)^{\frac{1}{n}} \quad (11)$$

3 Problem Descriptions

3.1 Finite Element Model. The pressure-reducing valve is composed of a valve body, four welded pipes, and a thermal seal that is placed inside of the valve. Dimensions and half geometry view of the pressure-reducing valve are shown in Table 1 and Fig. 1, respectively. The thermal seal was modeled for heat transfer analysis but removed for the creep cyclic plastic analysis since vulnerable locations against the thermomechanical loadings are the valve body rather than the seal, according to simulation results.

Three-dimensional solid element type, C3D8R, has been used to mesh the pressure-reducing valve in Abaqus (version 6.12-3) and a fully meshed model is presented in Fig. 2. Mesh sensitivity studies were carried out by comparing equivalent stress with a model meshed with an element type of C3D20R, which results confirm deviation of the stress magnitude less than 3%.

For boundary condition, a reference node is created at bottom center of the main pipe and kinematic coupling is applied between the reference node and bottom surface of the main pipe, which

Table 1 Pressure-reducing valve dimensions (mm)

	Outer radius	Inner radius	r/t ratio
Branch pipe	96.0	60.0	2.2
Flange pipe	158.2	91.9	1.9
Warming line	40.0	25.0	2.2
Main pipe	100.0	74.0	3.4

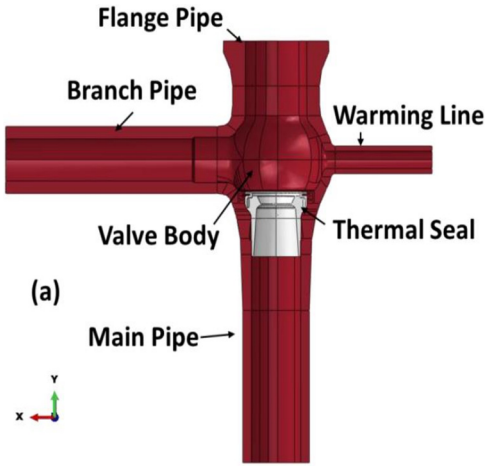

Fig. 1 The half geometry of the pressure-reducing valve

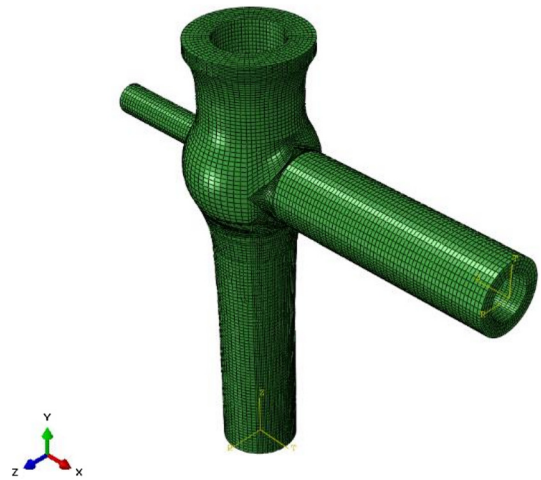

Fig. 2 Fully meshed model with three-dimensional solid elements

allows displacement in a radial direction of the main pipe but rest directions are fully constrained.

3.2 Material Properties. The pressure-reducing valve is made of Type 316 stainless steel. Physical properties and yield strength of the material are assumed to be the same as the previous research [14]. To simulate more realistic structural behavior, temperature dependent material properties are employed. The material properties applied for the finite element model is summarized in Table 2. For nonlinear behavior, elastic perfectly plastic model is considered.

For temperature related material properties, transient heat transfer model is developed with temperature dependent thermal conductivity and film coefficient for the startup period of 36000 s,

Table 2 Temperature dependent physical properties and yield strength of Type 316 stainless steel

Temperature (°C)	E (MPa)	υ	σ_y (MPa)
20	198,298	0.29	179.48
100	192,290		148.68
200	184,780		122.32
300	177,270		106.36
400	169,760		97.52
500	162,250		92.51
550	158,495		90.42

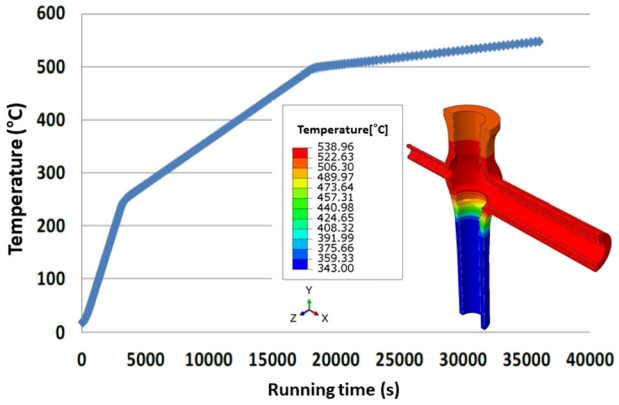

Fig. 4 Heat-transfer analysis results and temperature gradient of the pressure-reducing valve for startup period, 10 h

equivalent to 10 h, which analysis result is shown in Fig. 4. For predicting creep behavior, creep deformation model with power law is employed as Eq. (12) and Arrhenius law is used to implement temperature dependent creep deformation as Eq. (13)

$$\dot{\varepsilon}_{\text{creep}} = A^* t^m \sigma^n \tag{12}$$

$$A^* = A \cdot \exp\left(-Q/RT\right) \tag{13}$$

where A^*, m, n are the creep parameters; t is the dwell time; σ is the equivalent dwell stress; A is material constant; Q is the activation energy; R is the gas constant; T is the absolute temperature [K]. Parameters related to the temperature dependent creep deformation are summarized in Table 3.

3.3 Cyclic Thermomechanical Loadings. The pressure-reducing valve has experienced following cyclic thermomechanical loadings: system moments, internal pressures, and thermal loads. The system moment has come from pipelines connected before the branch pipe. The system moment consist of in-plane bending, out-of-plane bending, and torsional moment. Figure 3 presents the applied system moments and pressures. To implement the system moment, a reference node is created at center of the branch pipe end and kinematic coupling is connected between the node and the branch pipe end surface, which allows radial expansion only. Referenced system moments and torsion are calculated from Eqs. (14) and (15)

$$M_0 = \frac{4}{3}\sigma_y\left(R_0^3 - R_i^3\right) \tag{14}$$

$$T_r = \tau_{\max} \cdot \frac{J_T}{r_{\text{mean}}} \tag{15}$$

where M_0 is the limit bending moment of thick walled pipe; σ_y is the yield strength of the material; R_0 and R_i are the radius of the thick walled pipe, respectively; T_r is the limit torque; $\tau_{\max}$ is the

Table 3 Material properties for temperature dependent creep deformation for Type 316 stainless steel

Parameter	Value	Temp.(°C)
m	–0.587	540
n	4.1578	540
A	1.509×10^8	n/a
Q (J)	314,000	540
R (J·mol^{-1}·K^{-1})	8.31	n/a

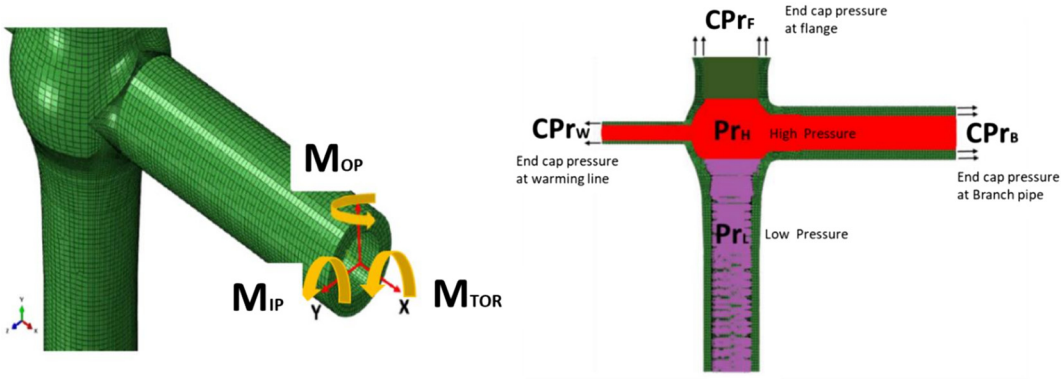

(*a*) (*b*)

Fig. 3 Applied mechanical loadings: (*a*) bending and torsional moments at branch pipe and (*b*) internal pressures and end cap pressures

Table 4 Applied pressure loading and system moment loadings

Loading	Pressure (MPa)	Loading	Moments (Nmm)
Pr_H	19.10	M_{IP}	8.06×10^7
Pr_L	5.31	M_{OP}	8.06×10^7
CPr_F	3.31	M_{TOR}	8.52×10^7
CPr_B	12.24		
CPr_W	12.24		

maximum shear strength of the material; J_T is the torsion constant for the section; r_{mean} is the mean radius of the pipe section.

Internal pressures taking place during the startup period are taken for normal operating condition of a supercritical boiler system. Figure 3(*b*) presents the inside of the pressure-reducing valve locations where the pressurized steam applied. All pipe ends are assumed as closed-end condition, which results in end-cap pressure acting on all pipe ends subjected to high pressure. End-cap pressure at the flange pipe has considered the effect of the end-cap pressure at the main pipe. The end-cap pressures are calculated from Eq. (16).

$$\sigma_l = \frac{p_i r_i^2 - p_o r_o^2}{r_o^2 - r_i^2} \tag{16}$$

where σ_l is the end-cap pressure; p_i and p_o are internal pressure and external pressure of the thick walled pipeline, respectively; r_i and r_o are the inside radius and outside radius of the thick walled pipeline, respectively. The calculated system moments and pressures are summarized in Table 4

Thermal loading is obtained by a transient heat analysis as shown in Fig. 4. Initial temperature is assumed as room temperature of 20 °C. During the startup period, the maximum temperature reaches up to 550 °C over high pressurized steam path line from the branch pipe to warming line. When the pressure–reducing valve activates, high pressurized steam with high temperature cool down by water spray inside of the valve body and the temperature and pressure are lowered to 350 °C and 5.3 MPa, respectively, and going into the startup vessel through the main pipe.

Loading cyclic is designed as Fig. 5. In creep cyclic plastic analysis, both the referenced pressure loading and thermal loading are applied as from 0.0 to 1.0, which are the normalized value. To evaluate the effect of individual system moment, each system moment with normalized value of 1.0 is applied together with the thermal and pressure loadings. In addition, the effect of the system moment on the structural integrity of the pressure-reducing valve is assessed for changes in the system moment from normalized value of 0.1 to of 0.4 with the pressure and thermal loadings.

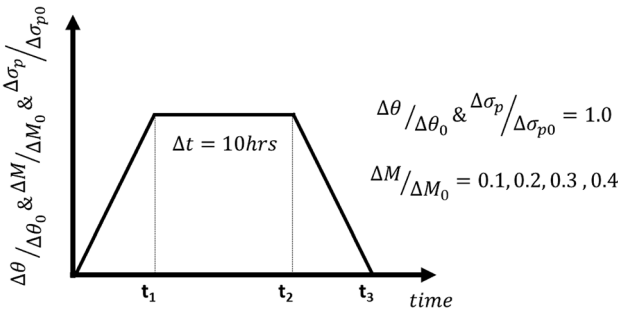

Fig. 5 Applied loading waveform under loading (t_1) - dwell (t_2) - unloading (t_3) cyclic loading for startup period, 10 h

4 Numerical Results and Discussions

4.1 Linear Elastic and Cyclic Plastic Behaviour. Linear elastic behavior and cyclic plastic behavior of the pressure-reducing valve under the same thermomechanical loading were presented by a previous study [14]. As it can be seen in Fig. 6, inside crotch corner of the pressure-reducing valve develops the maximum equivalent stress against the pressure and thermal loading. Whereas the system moment induces the maximum equivalent stress at outside of weldment connected between the branch pipe and valve body. For all thermomechanical loading applied, the maximum equivalent stress takes place at lower weldment zone of the branch pipe to the valve body.

The previous study also showed cyclic plastic analysis of the pressure-reducing valve against the thermos-mechanical loading and revealed an elastic shakedown boundary is identical to a plastic collapse limit, since primary stress dominate the developed equivalent stress. As shown the plastic collapse limit in Fig. 7, when the pressure-reducing valve is subjected to normalized cyclic thermal and pressure value of 1.0, the maximum normalized cyclic system moment must be less than 0.45, otherwise plastic collapse will occur. Hence, the effect of the system moment on creep-cyclic plastic behavior is assessed for the normalized system moment up to 0.4.

4.2 Creep Cyclic Plastic Behavior. To evaluate effects of an individual system moment on structural integrity of the pressure-reducing valve, creep cyclic plastic analysis is carried out against cyclic moment with normalized value of 0.3 for a dwell time of 10 h. Figure 8 shows creep deformation contours against the individual moment effect. Critical locations with creep deformation are observed from inside upper crotch corner of warming line, inside upper crotch corner of branch pipe, and outside weldment

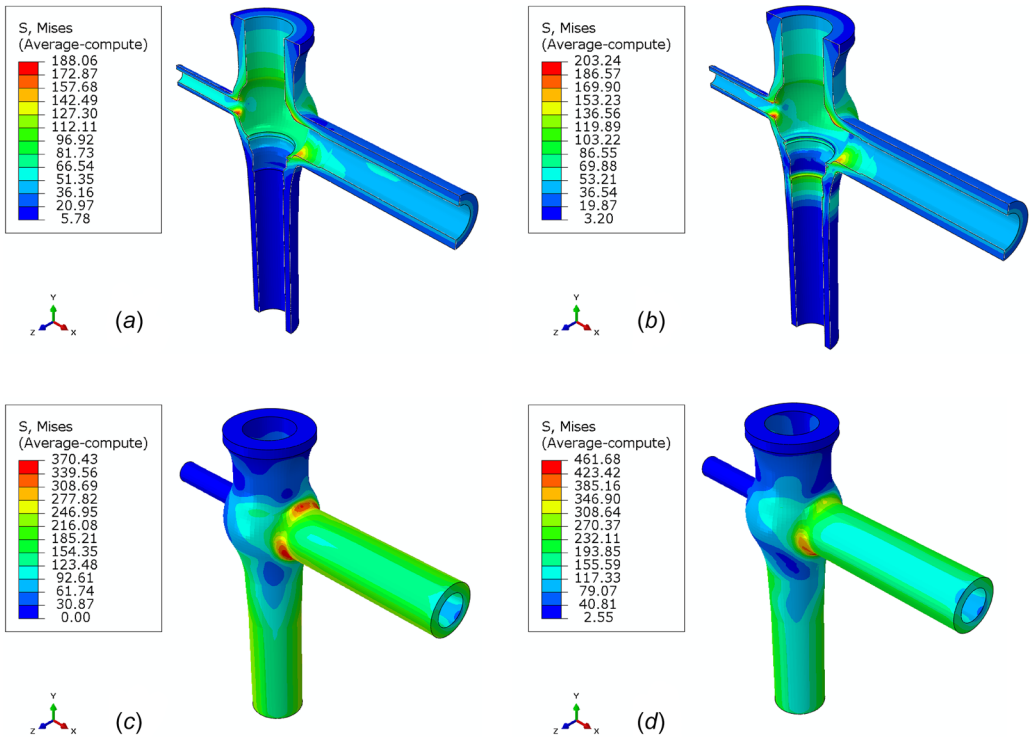

Fig. 6 Elastic behavior of the pressure-reducing valve against applied loadings: (*a*) internal pressure only, (*b*) internal pressure and thermal loading, (*c*) system moment loading only, and (*d*) all thermomechanical loadings

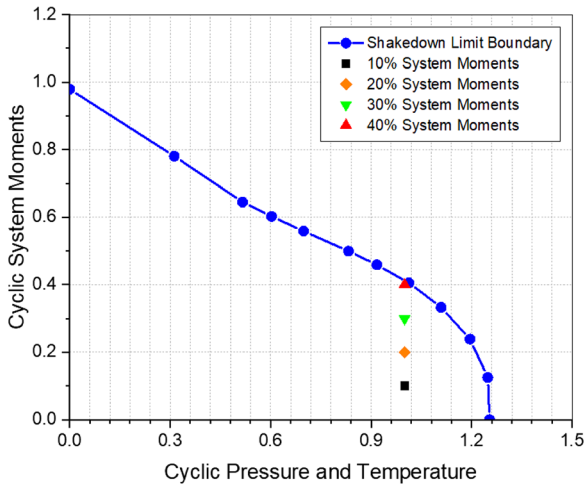

Fig. 7 Elastic shakedown limit boundary of the pressure reducing valve against the cyclic thermomechanical loading

of branch pipe against in-plane, out-of-plane, and torsional moment, respectively.

It can be seen from the simulation results that significant creep deformation does not develop per cycle. Creep deformation per cycle is larger in order of out-of-plane moment, in-plane moment, and torsional moment. Maximum total deformation occurs at the same location as the maximum creep deformation takes place and larger in order of in-plane moment, torsional moment, and out-of-plane moment. Table 5 presents summarized equivalent stress history, creep deformation and total deformation per cycle.

As it can be seen from Table 5, no yielding occurs at both loading and unloading periods, resulting in no plastic deformation developed except the inelastic creep deformation over a cycle. Figure 9 depicts stress–strain hysteresis loop of the critical location with creep deformation against the individual system moment loading.

It is worth mentioning that there is no apparent stress relaxation during a dwell period. This type of relaxation can take place when the primary stress has more effects on the PRV than the secondary stress. For instance, let's assume that both primary stress in tension and secondary stress in compression are imposed on the PRV under thermomechanical loading. Combined equivalent stress

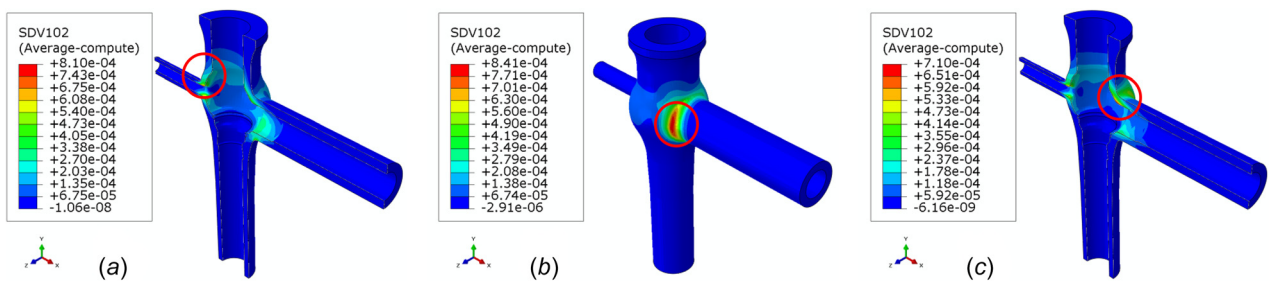

Fig. 8 Absolute creep strain per cycle with temperature dependent creep effects against cyclic system moment normalized as 0.3: (*a*) in-plane, (*b*) out-of-plane, and (*c*) torsional

Table 5 Equivalent stress history and creep deformation per cycle of the critical location, and total deformation per cycle against individual system moment case

System moment	Loading (MPa)	Creep (MPa)	Unloading (MPa)	Creep strain (abs)	Total strain (abs)
Inplane	87.97	88.66	–103.5	8.10×10^4	1.82×10^3
Out-of-plane	89.37	89.72	–54.87	8.41×10^4	1.74×10^3
Torsional	85.65	85.66	–82.65	7.10×10^4	1.76×10^3

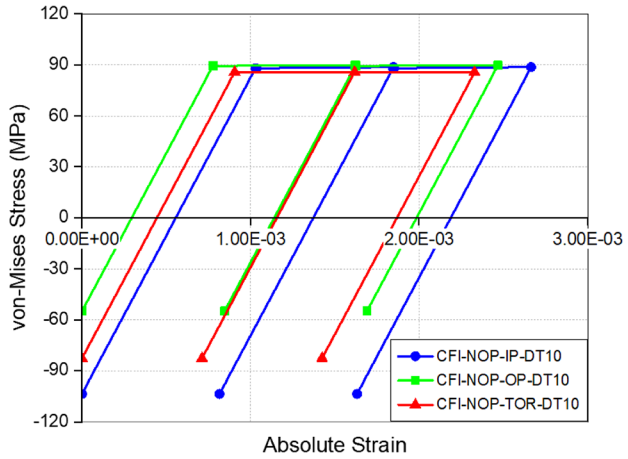

Fig. 9 Stress-strain hysteresis loop of critical location with creep deformation against individual system moments

level at loading instance can be reduced by the secondary stress. However, the compressive secondary stress begins to relax at creep instance, which leads to the primary stress in tension affects more to equivalent stress. The increase in dwell stress is a possible high temperature mechanism when rupture reference stress is higher than start of dwell stress, and they are introduced in R5 procedures [15] and other researches [10,16].

To evaluate the effects of the temperature dependent creep parameters on the creep-cyclic plasticity, structural response of the PRV is analyzed against the same cyclic system moment using the original LMM eDSCA that employees a temperature independent creep parameters (A = 2.70E-12; n = 4.1578; m=-0.587, at 540 °C).

Figure 10 depicts the overall creep deformation of the PRV with the effect of the temperature independent creep parameters against the individual cyclic system moments. The maximum creep strain occurs at the identical location to individual system moment effects shown in Fig. 8 but the amount of the deformation almost doubled. As can be seen in Fig. 4 the PRV has temperature gradient along with vertical direction not with through thickness, so that resultant thermal stress as Fig. 6(*b*) is developed over the connecting area between main pipe and valve body and flange pipe and valve body. Owing to the independent creep parameters it can be presumed that the PRV may experience exaggerated creep deformation with the relatively lower temperature area such as the connecting zone with the valve body, affecting to structural integrity of the PRV.

Another creep-cyclic plastic analysis is conducted to evaluate the effects of combined system moment level on structural integrity of the pressure-reducing valve. The level of the combined system moment increases from normalized value of 0.1 to 0.4 and the dwell time of 10 h is considered. Figure 11 presents creep deformation contour per cycle against the effects of combined system moment level. Maximum creep deformation take place at inside upper crotch corner of the warming line against the normalized combined system moment level up to 0.2 but it shifts to outside and then inside weldment of the branch pipe when the level reaches 0.3 and 0.4, respectively. Table 6 summarizes the equivalent stress history and creep deformation per cycle of the critical location, and maximum total deformation per cycle taken from the pressure-reducing valve.

The maximum total deformation takes place at the same location as the maximum creep deformation occurs when the moment level raise up to 0.2 but at different locations when the moment level is greater than 0.2. As can be seen from Table 6 the effect of the combined moment level on creep deformation per cycle is not substantial but significant impacts to total strain accumulation per cycle. This is because the pressure-reducing valve experiences yielding when subjected to the combined moment level over 0.3, which results in more than twice total strain accumulated at the moment level of 0.4 than of 0.3.

Figure 12 illustrates stress–strain hysteresis loops of critical locations against each moment level. As the same trend as the individual moment effects showed, primary stress dominates overall stress of the critical locations, resulting in stress relaxation not taking place during a dwell period. Moreover, as moment level increases, the critical locations tend to have larger creep deformation per cycle but smaller total deformation per cycle due to decrease in unloading stress level.

Overall, it is found out that out-of-plane moment develops the largest creep deformation per cycle among the three concerned system moments but amount of the creep deformation per cycle does not affect critically to structural integrity of the pressure-reducing valve under the given loading condition. In additions, as the moment level increases, the pressure-reducing valve experiences plastic deformation more than creep deformation. Hence it is

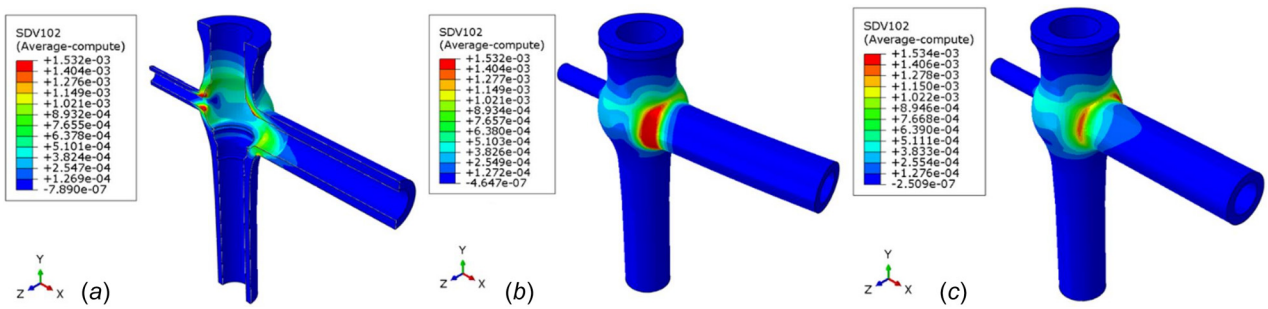

Fig. 10 Absolute creep strain per cycle with temperature independent creep effects against cyclic system moment normalized as 0.3: (*a*) in-plane, (*b*) out-of-plane, and (*c*) torsional

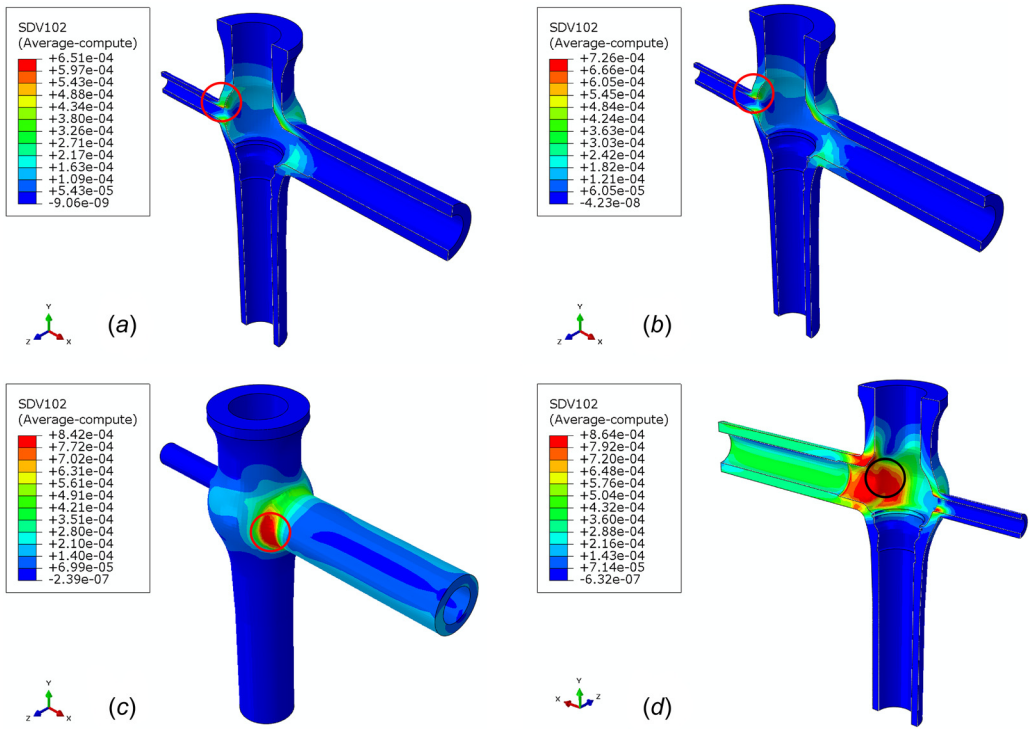

Fig. 11 Creep deformation per cyclic against the combined system moment level: (*a*) 10%, (*b*) 20%, (*c*) 30%, and (*d*) 40%

Table 6 Equivalent stress history and creep deformation per cycle of the critical location, and total deformation per cycle against normalized combined system moment

Combined moment (%)	Loading (MPa)	Creep (MPa)	Unloading (MPa)	Creep strain (abs)	Total strain (abs)
10	84.46	85.19	–93.9	6.51×10^4	1.80×10^3
20	84.72	87.34	–98.32	7.26×10^4	1.92×10^3
30	87.75	91.63	–45.08	8.42×10^4	2.22×10^3
40	88.26	91.63	–18.51	8.64×10^4	5.12×10^3

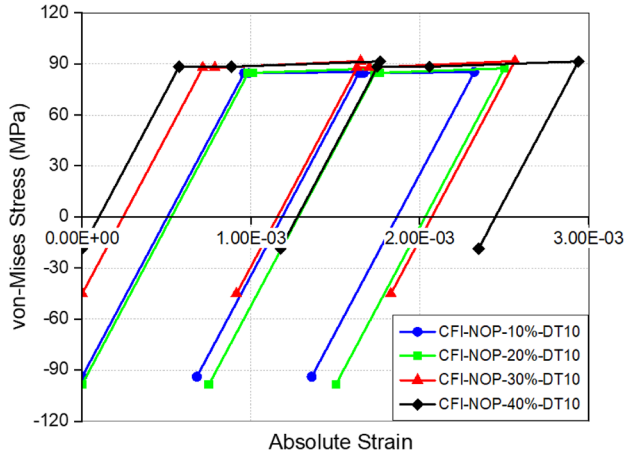

Fig. 12 Stress–strain hysteresis loop of critical location with creep deformation against combined system moments

predicted that fatigue failure is likely to occur rather than creep related failure at higher moment level.

5 Conclusions

Creep cyclic plastic analysis of the pressure-reducing valve was conducted against cyclic thermal load, cyclic internal pressure, and cyclic system moments (in-plane, out-of-plane, torsional) using the Linear Matching Method eDSCA. The effects of individual system moment and combined system moment level on structural integrity of the pressure-reducing valve were assessed and following numerical results have been obtained.

For the effect of the individual system moments, out-of-plane moment revealed the largest creep strain accumulated per cycle, but each moment developed a more or less the same total deformation per cycle. There was interesting point observed that no apparent stress relaxation occurred during a dwell period due to dwell stress dominated by primary stress. As shown stress–strain hysteresis loops per cycle in Fig. 9, it can be predicted that the structural integrity of the pressure-reducing valve may be threaten with the system moments, leading to creep enhanced ratchetting response. A comparative study on the effects of temperature dependents creep parameters revealed that structural integrity assessment with independent creep parameter predict more conservative creep deformation per cycle. Further parametric study was performed to evaluate the effect of the moment level on the structural integrity of the valve and presented that total deformation is attributed to plastic deformation more than creep deformation per cycle as the moment level increase. Hence it can be presumed that the pressure reducing valve is likely to experience crack due to fatigue damage rather than creep damage, when significant system moment is applied during operation.

This research presented potential high temperature failure mechanism of the pressure reducing valve that is generally attached in the main steam line of supercritical boiler system.

Assessment results demonstrated the effect of system moments on the integrity of the pressure reducing valve, which provide design engineer with insight into creep-cyclic plasticity of the valve under the complex loading. Moreover, this research showed the Direct Steady Cycle Analysis method can be an efficient analysis manner for detailed inelastic structural analysis.

Acknowledgment

The authors gratefully acknowledge supports from Engineering Analysis Services Limited, UK, during the course of this work.

Funding Data

- This study was supported by the Research Program funded by the SeoulTech (Seoul National University of Science and Technology; Funder ID: 10.13039/501100002553).

References

[1] Abe, F., 2016, "Progress in Creep-Resistant Steels for High Efficiency Coal-Fired Power Plants," ASME J. Pressure Vessel Technol., **138**(4), p. 040804.
[2] Cho, N.-K., Chen, H., Boyle, J., and Xuan, F.-Z., 2018, "Enhanced Fatigue Damage Under Cyclic Thermo-Mechanical Loading at High Temperature by Structural Creep Recovery Mechanism," Int. J. Fatigue, **113**, pp. 149–159.
[3] Giugliano, D., Barbera, D., Chen, H., Cho, N.-K., and Liu, Y., 2019, "Creep-Fatigue and Cyclically Enhanced Creep Mechanisms in Aluminium Based Metal Matrix Composites," Eur. J. Mech. A/Solids, **74**, pp. 66–80.
[4] Ainsworth, R., 2003, "British Energy Generation Ltd," R5: Assess. Procedure High Temperature Response Structures, vol. **3**, British Energy Generation Ltd, London, UK.
[5] ASME, 2015, *Section III-Rules for Construction of Nuclear Facility Components-Division 2-Code for Concrete Containments*, ASME, New York, Standard No. BPVC-III-2 - 2021.
[6] RCC-MRx, A., 2013, *Code of Design and Construction Rules for Mechanical Component in Nuclear Installations*, AFCEN, Courbevoie, France.
[7] Chen, H., Ponter, A., and Ainsworth, R., 2006, "The Linear Matching Method Applied to the High Temperature Life Integrity of Structures. Part 1. Assessments Involving Constant Residual Stress Fields," Int. J. Pressure Vessels Piping, **83**(2), pp. 123–135.
[8] Chen, H., and Ponter, A., 2005, "Integrity Assessment of a 3D Tube-plate Using the Linear Matching Method. Part 1. Shakedown, Reverse Plasticity and Ratchetting," Int. J. Pressure Vessels Piping, **82**(2), pp. 85–94.
[9] Chen, H., and Ponter, A., 2006, "Linear Matching Method on the Evaluation of Plastic and Creep Behaviours for Bodies Subjected to Cyclic Thermal and Mechanical Loading," Int. J. Numer. Methods Eng., **68**(1), pp. 13–32.
[10] Cho, N.-K., Wang, R.-Z., Ma, Z., Chen, H., and Xuan, F.-Z., 2019, "Creep-Fatigue Endurance of a Superheater Tube Plate Under Non-Isothermal Loading and Multi-Dwell Condition," Int. J. Mech. Sci., **161–162**, p. 105048.
[11] Cho, N.-K., Chen, H., Mackenzie, D., and Giugliano, D., 2020, "Investigating the Effects of Cyclic Thermo-Mechanical Loading on Cyclic Plastic Behavior of a Ninety-Degree Back-to-Back Pipe Bend System," ASME J. Pressure Vessel Technol., **142**(2), p. 021301.
[12] Zheng, X., Chen, H., Ma, Z., and Xuan, F.-Z., 2019, "A Novel Fatigue Assessment Approach by Direct Steady Cycle Analysis (DSCA) Considering the Temperature-Dependent Strain Hardening Effect," Int. J. Pressure Vessels Piping, **170**, pp. 66–72.
[13] Ma, Z., Chen, H., Liu, Y., and Xuan, F.-Z., 2020, "A Direct Approach to the Evaluation of Structural Shakedown Limit Considering Limited Kinematic Hardening and Non-Isothermal Effect," Eur. J. Mech. A/Solids, **79**, p. 103877.
[14] Cho, N.-K., Pavitra, B., and Hurst, A. M., 2020, "Investigating Structural Response of Pressure Reducing Valve of Supercritical Steam Generator System Under Cyclic Moments, Thermal Transient, and Pressure Loadings," ASME Paper No. ICONE2020-16426.
[15] Ainsworth, R., Budden, P., and Hales, R., 1996, "Assessment of the High-Temperature Response of Structures: Developments in the R5 Procedure," Proceedings of Creep and Fatigue. Design and Life Assessment at High Temperature, **6**th International Conference on Creep and Fatigue, London, UK, Apr. 15–17, pp. 385–397.
[16] Giugliano, D., Cho, N.-K., Chen, H., and Gentile, L., 2019, "Cyclic Plasticity and Creep-Cyclic Plasticity Behaviours of the SiC/Ti-6242 Particulate Reinforced Titanium Matrix Composites Under Thermo-Mechanical Loadings," Compos. Struct., **218**, pp. 204–216.